AIAA 2003-2131

Opening Loads Analyses for Various Disk-Gap-Band Parachutes

J. R. Cruz
NASA Langley Research Center
Hampton, VA

M. Kandis and A. Witkowski
Pioneer Aerospace
South Windsor, CT

17th AIAA Aerodynamic Decelerator Systems Technology Conference and Seminar
19–22 May 2003
Monterey, California

OPENING LOADS ANALYSES FOR VARIOUS DISK-GAP-BAND PARACHUTES

Juan R. Cruz*
NASA Langley Research Center
Hampton, Virginia

Mike Kandis† and Allen Witkowski‡
Pioneer Aerospace Corporation
South Windsor, Connecticut

ABSTRACT

Detailed opening loads data is presented for 18 tests of DGB parachutes of varying geometry with nominal diameters ranging from 43.2 to 50.1 ft. All of the test parachutes were deployed from a mortar. Six of these tests were conducted via drop testing with drop test vehicles weighing approximately 3,000 or 8,000 lb. Twelve tests were conducted in the National Full-Scale Aerodynamics Complex 80- by 120-foot wind tunnel at the NASA Ames Research Center. The purpose of these tests was to structurally qualify the parachute for the Mars Exploration Rover mission. A key requirement of all tests was that peak parachute load had to be reached at full inflation to more closely simulate the load profile encountered during operation at Mars. Peak loads measured during the tests were in the range from 12,889 to 30,027 lb. Of the two test methods, the wind tunnel tests yielded more accurate and repeatable data. Application of an apparent mass model to the opening loads data yielded insights into the nature of these loads. Although the apparent mass model could reconstruct specific tests with reasonable accuracy, the use of this model for predictive analyses was not accurate enough to set test conditions for either the drop or wind tunnel tests. A simpler empirical model was found to be suitable for predicting opening loads for the wind tunnel tests to a satisfactory level of accuracy. However, this simple empirical model is not applicable to the drop tests.

SYMBOLS AND ACRONYMS

A	wind tunnel cross sectional area at the test section
A_D	disk area
$A_{V,c}$	constrained vent area
C_DS	parachute drag area
C_{D_0}	parachute steady-state drag coefficient for a fully inflated parachute
C_x	opening load factor
D_B	band diameter
D_D	disk diameter
$D_{V,c}$	constrained vent diameter
D_0	nominal parachute diameter
F_p	force generated by the parachute during inflation
g	acceleration of gravity
H_B	band height
H_G	gap height
k_0	nondimensional constant used in the calculation of the parachute apparent mass
L_S	suspension lines length
m_a	parachute apparent mass
m_p	parachute physical mass
q	dynamic pressure
q_{eff}	effective dynamic pressure
q_∞	dynamic pressure in the wind tunnel far upstream of the parachute canopy
S_p	projected parachute area
$S_{p_{max}}$	maximum projected parachute area
S_r	parachute projected area ratio
S_0	nominal parachute area
t	time
t_{inf}	inflation time from start of inflation to full inflation
V	velocity (airspeed)
V_{eff}	effective velocity (airspeed)
V_∞	airspeed in the wind tunnel far upstream of the parachute canopy
$\lambda_{g,c}$	geometric porosity based on the constrained vent area
Γ_0	volume of a hemisphere with diameter equal to D_0
ρ	fluid density

DGB	Disk-Gap-Band
DTST	Drop Test
DTV	Drop Test Vehicle
FI	Full Inflation
SI	Start of Inflation
LS	Line Stretch
MER	Mars Exploration Rover
MF	Mortar Firing

*Aerospace Engineer, Juan.R.Cruz@nasa.gov
†Analytical Engineer, mkandis@pioneer.zodiac.com
‡Engineering Program Manager, awitkowski@pioneer.zodiac.com, Member AIAA

MSL Mean Sea Level
NFAC National Full-Scale Aerodynamics Complex
PL Peak Load
WTMD Wind Tunnel Mortar Deployment

INTRODUCTION

The structural qualification of the parachute for the Mars Exploration Rover (MER) mission[1,2] was conducted through a combination of full-scale low-altitude drop tests[3,4] and wind tunnel tests in the National Full-Scale Aerodynamics Complex (NFAC) 80- by 120-foot wind tunnel at the NASA Ames Research Center.[5] The parachute used by MER is of the Disk-Gap-Band (DGB) design developed for the Viking mission[6] in 1976 and used on several other missions including Mars Pathfinder[7,8] in 1997. As with prior missions,[9] the MER parachute will be deployed by a mortar.[10]

The primary objective of the tests discussed herein was to show compliance with the MER parachute's structural qualification requirement. For the MER mission, this requirement stated that the parachute had to withstand a load 25 percent greater than the calculated maximum opening load at Mars without sustaining damage that would affect parachute performance. The maximum predicted opening load at Mars, including various safety factors and allowances for uncertainties, was calculated to be 19,360 lb. This resulted in a peak load qualification requirement of 24,200 lb for the MER parachute. During Mars operation, parachute inflation occurs under near-infinite mass conditions resulting in an almost constant dynamic pressure during the parachute deployment and inflation. As a consequence the peak opening load during Mars operation occurs when the parachute reaches full inflation. Thus, an additional requirement for the structural qualification tests was that the peak opening load had to occur at full inflation. It should be noted that these tests were only approximations of the conditions to be encountered at Mars. It was not feasible to reproduce all of the MER mission parameters of importance. All tests were conducted at low altitudes on Earth and at subsonic speeds. On Mars the parachute will be deployed at supersonic speeds in a low-density atmosphere (approximately two orders of magnitude less dense than Earth's atmosphere at sea level). A discussion of the factors relevant to the testing and qualification of parachutes at low altitudes on Earth and subsonic speeds, when the intended operation is in a low-density atmosphere at supersonic speeds, is given in reference 11.

The ability to predict the peak opening load, and the point in time at which it occurs during parachute inflation, was key to the design and execution of both the drop and wind tunnel tests conducted in support of the MER structural qualification program. During the design of the drop test vehicles (DTV), opening loads analyses of various types (including those described later in this paper) were used to determine the mass required to achieve peak opening load at full inflation, as well as the time from DTV release to mortar fire needed to obtain the desired peak load. Those predictions were hampered by lack of a suitable analysis. Predicting the opening loads during the full-scale wind tunnel tests was somewhat simpler, since the wind tunnel provides an almost constant and predictable dynamic pressure during parachute inflation.

The objective of this paper is to present the opening loads data and retrospective analyses for the MER parachute drop and wind tunnel structural qualification tests. This information can provide insights into opening loads analyses at subsonic speeds that may be useful for future programs using similar DGB parachutes. Although results are presented for both the drop and wind tunnel tests, more emphasis is placed on the latter because the data obtained during the wind tunnel test series was more accurate and thus easier to interpret.

An understanding of, and the ability to model unsteady aerodynamic forces was critical to the opening loads analyses. The apparent mass model used to analyze the data is presented in the next section. This model is based on the separation of opening loads into two components: the first due to steady-state drag forces and the second due to apparent mass effects. Modification of this analysis to account for wind tunnel blockage effects, for use in analyzing the wind tunnel test data, is also presented. This is followed by a presentation of the data and analyses for the drop tests and the wind tunnel tests. Comparisons of the results for these two test programs are also discussed. Finally, an assessment of the suitability of the analytical model to predict opening loads is presented.

ANALYTICAL FRAMEWORK

The equations used to analyze the data are a variant of those presented by McEwan,[12] with the main differences appearing in how the apparent mass and steady state drag force are modeled. During a vertical drop, following mortar deployment of the parachute, the force generated by the parachute on the DTV from

the start of inflation[§] to full inflation, F_p, is assumed to be given by:

$$F_p = qC_D S + \frac{d}{dt}\left\{\left(m_a + m_p\right)V\right\} - m_p g \qquad (1)$$

where q is the dynamic pressure, $C_D S$ is the parachute drag area, t is time, m_a is the apparent mass (due to the fluid), m_p is the physical mass of the parachute, V is the velocity (assumed to be equal to the airspeed), and g is the acceleration of gravity.[¶] Performing the indicated differentiation yields:

$$F_p = qC_D S + (m_a + m_p)\frac{dV}{dt} + \frac{dm_a}{dt}V - m_p g \qquad (2)$$

The apparent air mass is assumed to be described by:

$$m_a = k_0 \rho \Gamma_0 S_r^{3/2} \qquad (3)$$

where ρ is the fluid density and Γ_0 is the volume of a hemisphere with a diameter equal to the nominal diameter of the parachute, D_0: $\Gamma_0 = \pi D_0^3/12$. S_r is the parachute projected area ratio, a nondimensional ratio, $S_r = S_p/S_{p_{\max}}$, where S_p is the projected parachute area at a given point in time during the inflation and $S_{p_{\max}}$ is the maximum projected parachute area. The constant k_0 is nondimensional. Performing the differentiation for m_a indicated in equation 2 results in:

$$\frac{dm_a}{dt} = k_0 \frac{d\rho}{dt}\Gamma_0 S_r^{3/2} + \frac{3}{2}k_0 \rho \Gamma_0 S_r^{1/2}\frac{dS_r}{dt} \qquad (4)$$

The term $C_D S$ is approximated as:

$$C_D S = C_{D_0} S_0 S_r \qquad (5)$$

where C_{D_0} is the steady-state parachute drag coefficient for a fully inflated parachute and S_0 is the nominal parachute area. Substituting equations 3, 4, and 5 into equation 2, and neglecting terms involving m_p and $d\rho/dt$ since they are small as compared to the other terms over the time period of interest, yields the basic equation for the analysis of the test data and calculation of opening loads:

$$F_p = qC_{D_0} S_0 S_r + k_0 \rho \Gamma_0 S_r^{3/2}\frac{dV}{dt} + \frac{3}{2}k_0 \rho \Gamma_0 S_r^{1/2}\frac{dS_r}{dt}V \qquad (6)$$

Using test data from various sources, one can determine all quantities in equation 6 except for k_0. Since the peak opening load is of greatest interest, substituting the appropriate values of the various quantities into equation 6 at peak opening load allows for the determination of k_0. Having identified a value for k_0, an analytical reconstruction of a given test that yields the same peak opening load as the test data can be generated. However, the reconstruction between the start of inflation and full inflation will only be approximate due to the simplicity of the model and various measurement uncertainties. Predictive analyses for another test can be conducted with this value of k_0 and the associated S_r vs time curve.

It is realized that equation 6 represents an approximate model for a problem of greater physical complexity. However, the expectation is that enough flexibility is available in this approximate model to yield predictions of engineering value when calibrated with relevant experimental data.

ADJUSTMENTS FOR WIND TUNNEL TESTS

When performing parachute tests in a wind tunnel, the effect of wind tunnel blockage must be accounted for. This blockage increases the effective velocity and dynamic pressure experienced by the canopy. In the present investigation the effective velocity, V_{eff}, and effective dynamic pressure, q_{eff}, are used in place of V and q for analyzing the data obtained from wind tunnel tests. The methods used to determine V_{eff} and q_{eff} are discussed in this subsection.

Prior wind tunnel tests of the Space Shuttle Orbiter ribbon parachute[13] conducted in the 80- by 120-foot test section of NFAC, found that the following blockage equation yielded good results:

$$q_{eff} = q_\infty + 1.85\frac{F_p}{A} \qquad (7)$$

where q_∞ is the wind tunnel dynamic pressure far upstream of the parachute canopy and A is the wind tunnel cross sectional area at the test section which was assumed to be 9,600 ft^2 for the 80- by 120-foot wind tunnel[#] (note that the notation here is somewhat different from that used in reference 13). This equation was based on work performed by Macha and Buffington[14] and derived under the assumption of steady-state conditions. Tests performed by the MER team[5] validated its applicability to DGB parachutes

[§] *Start of inflation* is used to refer to the point where the load is at a minimum following the snatch load.

[¶] *Force* is used to denote aerodynamic forces; *load* is used to denote both aerodynamic forces and forces of other origins (e.g., mortar recoil, snatch).

[#] The actual cross sectional area of the tunnel is slightly smaller due to an acoustic lining around the test section.

under steady-state conditions. In the present investigation the conditions are dynamic: as the parachute inflates blockage increases over a time scale of several seconds. Given that the blockage arises due to parachute inflation (with a corresponding increase in projected area), F_p in equation 7 was replaced by $q_{eff} C_{D_0} S_0 S_r$ in the present investigation. Solving the resulting equation for q_{eff} yields:

$$q_{eff} = \frac{q_\infty}{1 - 1.85 \frac{C_{D_0} S_0 S_r}{A}} \tag{8}$$

V_{eff} can then be determined from:

$$V_{eff} = \sqrt{\frac{2 q_{eff}}{\rho}} \tag{9}$$

When analyzing or predicting the outcome of a wind tunnel test, q and V in equation 6 were replaced by q_{eff} and V_{eff}, respectively. During the wind tunnel tests conducted under the present investigation, q_∞ was almost constant from the start of inflation to full inflation. The changes in q_{eff} and V_{eff} were almost entirely due to blockage effects as the parachute inflated.

Two key points need to be emphasized regarding the blockage correction. First, equation 7 was validated for steady-state test conditions. Its use in the present investigation for dynamic conditions is an extrapolation that has not been validated. Second, replacing F_p in equation 7 by $q_{eff} C_{D_0} S_0 S_r$ to yield equation 8 was done to avoid unrealistic blockage effects. Since F_p at full inflation is significantly greater than the steady-state drag of the parachute just a fraction of a second earlier, equation 7 yielded high values of the blockage at full inflation. These values were deemed to be unrealistic - calculating blockage by equation 8 yielded more plausible values without a high rate of change in blockage near full inflation. Given that the inflated parachute changed little in projected diameter from peak load to a fraction of a second later,[**] the behavior predicted by equation 8 is more plausible.

DROP TESTS

Six tests were conducted during the drop test series. These tests were denoted by DTST (Drop Test) and a three digit number: DTST 037, DTST 038, DTST 040, DTST 049, DTST 050, and DTST 071.

[**] Due to their construction, MER DGB parachutes did not experience significant over-inflation.

TEST PARACHUTES

All parachutes used in the drop test series were geometrically similar to that used for the Mars Pathfinder mission[7,8] and thus were classified to be of the MPF type. This parachute type is a modified version of that used by Viking.[6] The changes from the Viking type are mainly in the ratios of band height, gap height, and vent diameter to nominal diameter. The design nominal diameter, D_0, of the parachutes used during the drop test series was 49.5 ft. Construction details for these parachutes are given in table 1. Minor structural variations existed between these test parachutes. All parachutes were pressure packed to a density of approximately 45 lb/ft^3 in bags suitable for mortar deployment.

TEST SETUP AND PROCEDURES

DROP TEST VEHICLES AND INSTRUMENTATION

One of the drop test vehicles is shown in figure 2. It consists of a cylindrical/conical steel nose (serving as ballast and accounting for most of the DTV's weight), a cylindrical aluminum body, and large wire-braced fins fabricated from aluminum honeycomb sheet. The cylindrical body served to house most of the instrumentation and the mortar. This DTV design minimized the vehicle's mass moments of inertia, thus maximizing the effect of aerodynamic forces and reducing the total angle of attack at mortar firing. The fins were considered to be expendable and were replaced as necessary after each test. The steel nose and the cylindrical body suffered little to no damage after each test, and were re-used with minimal refurbishing. Two versions of the DTV were used: one with a nominal weight of 3,000 lb and a second with a nominal weight of 8,000 lb. A more detailed description of the design of the DTV is given in reference 4.

The instrumentation most relevant to this study were the accelerometers and digital video cameras. Two sets of accelerometers were mounted to the DTV. A Crossbow VG400CB-200 gyroscope provided accelerometer data with respect to three mutually orthogonal axes. This gyroscope had an accelerometer range of ±10 g in each axis. Data from the Crossbow VG400CB-200 was stored in an on-board digital data logger using a 12-bit analog-to-digital converter. The uncertainty associated with this combination of accelerometer and analog-to-digital converter was ±0.11 g. The second set of acceleration measurements was provided by a Crossbow CXL10P3 accelerometer device. Accelerations along three mutually orthogonal axes, with a range of ±10 g in each axis, were obtained

from this device and recorded in an on-board digital data logger using a 8-bit analog-to-digital converter. The uncertainty associated with this combination of accelerometer and analog-to-digital converter was ±0.26 g. Both the 12- and 8-bit data loggers recorded data at 200 Hz. For all but one of the drop tests (DTST 071), the data from the Crossbow VG400CB-200 stored in the 12-bit data logger were used in the analyses presented in this paper because of its higher accuracy. For drop test DTST 071 the data from the CXL10P3 stored in the 8-bit data logger was used in the analyses presented in this paper (the data from the VG400CB-200 stored in the 12-bit data logger for DTST 071 was corrupted due to landing damage). The accelerometer data were used to calculate loads, DTV velocity and altitude (by integrating the accelerometer data), and dynamic pressure (by combining the calculated velocity and altitude with the appropriate atmospheric sounding data). In addition, accelerometer data were used to determine the timing of key events such as mortar firing. Note that the accelerometers were selected for the determination of loads. They were adequate for this purpose. However, the analyses presented in this paper required additional information. Although a best effort was made to derive accurate velocities and dynamic pressures as described above, these quantities had significant uncertainties. This should be kept in mind when considering the results of analyses that follow. Additional relevant data was obtained from two aft-facing digital video cameras mounted on the DTV cylindrical body. These digital video cameras recorded at 30 frames per second. Data from these video cameras were used to determine S_r. Digital video cameras operated by observers on the ground yielded additional timing information of key test events. There was additional instrumentation on the DTV (e.g., angle of attack and sideslip vanes and transducers), but the data generated was not directly related to the subject matter of this paper (i.e., opening loads).

TEST PROCEDURES

Drop testing was conducted at the Idaho Army National Guard Orchard Training Range south of Boise, Idaho. The DTV was assembled in the hangar and secured to a launch cradle that held it vertically. The instrumentation was then installed and checked. A packed parachute was placed in the mortar mounted on the cylindrical body of the DTV. The fully assembled DTV, on its launch cradle, was then transported to the drop zone. The mortar gas generator was installed at the test site. After starting all video cameras and connecting the lifting cable and release to the DTV, a helicopter lifted the DTV to the desired release altitude. Once stabilized at the required altitude, the DTV was released at the command of the test coordinator. Data logger recording was initiated upon release. At a pre-set time following release the mortar was fired by an on-board timing sequencer, deploying the parachute. The time from release to mortar firing was calculated and set based the desired peak opening load for each test. Upon landing, the parachute was secured and removed from the DTV. All recording instruments were then turned off and removed for downloading of data. The DTV was then reloaded on its launch cradle for transportation back to the hangar where it was refurbished as necessary and prepared for the next test.

RESULTS AND ANALYSES

Six tests were conducted during the drop test series. The first two tests (DTST 037 and 038) were conducted with a DTV of 3,000 lb nominal weight, whereas the final four tests (DTST 040, 049, 050, and 071) were conducted with a DTV of 8,000 lb nominal weight. A summary of the drop test results is given in table 2.

It became evident after the first two drop tests that it was impossible to achieve the desired peak load at full inflation for these parachutes (a test requirement) with the 3,000 lb DTV – the weight was insufficient to yield this outcome. As can be seen from table 2, peak load for both of these tests occurred at a time approximately 66 percent from the start of inflation to full inflation. A second lower load peak occurred at full inflation. Figure 3 shows the load, dynamic pressure, and parachute projected area ratio vs time for DTST 038 with key events identified. The non-dimensional projected area ratio, S_r, is shown increasing from zero to one during the inflation time (S_r is multiplied by 10 in this and subsequent figures to make it visible in the same scale as q). At mortar firing, the DTV was accelerating and the dynamic pressure was increasing. As the parachute inflated, the parachute drag force began reversing the DTV acceleration, causing the dynamic pressure to reach a peak value and then drop rapidly. This resulted in a lower dynamic pressure at full inflation than experienced earlier in the inflation process. Under these conditions, the combination of dynamic pressure, parachute drag area, and unsteady aerodynamic forces resulted in the peak load occurring prior to full inflation. After examining the data from DTST 037 and 038, it was decided to increase the weight of the DTV to 8,000 lb for subsequent tests. By doing this, the deceleration caused by the parachute during the inflation process would be reduced, thereby limiting the decrease in the dynamic pressure, and yielding the desired peak load at full inflation.

The four additional drop tests (DTST 040, 049, 050, and 071) were conducted using the 8,000 lb DTV. All four of these tests yielded peak loads at full inflation.

Figure 4 shows load, dynamic pressure, and parachute projected area ratio vs time for DTST 040. Although the dynamic pressure decreased from its peak value, the drop was not sufficient to cause the peak load to occur before full inflation. The observed plateau in the load profile is attributed to a hesitation in the parachute inflation as seen in the S_r curve. A plot of peak load vs mortar firing time, as shown in figure 5 highlights the key difficulty encountered in undertaking the drop test series: predicting the peak opening load. The correlation between peak load and mortar firing time was poor. For example, a comparison of the results from DTST 040 and DTST 049 indicated that two tests with significantly different mortar firing times; 3.10 and 2.32 seconds, yielded essentially the same peak load; 29,731 and 29,518 lb (see table 2). During the drop test program, predicting the required mortar firing time to achieve a desired peak load was accomplished by applying simple drag-area models and the apparent mass model to the available data. The accuracy of these predictions was poor – drop tests often resulted in peak loads very different from those desired. This was in sharp contrast to wind tunnel testing (described in the next section) where load prediction by a simple empirical method yielded more accurate and consistent results. The non-dimensional inflation distances obtained from these four tests, as shown in table 2, were fairly consistent, varying from 7.93 to 9.12 nominal diameters, with an average of 8.60.

Apparent mass model reconstructions and test data for the four drop tests conducted with the 8,000 lb DTV (i.e., DTST 040, 049, 050, and 071) are shown in figures 6 through 9. Note that the results are plotted against non-dimensional time, t/t_{inf}, where t_{inf} is the inflation time from the start of inflation to full inflation (also peak load for these tests), and time t is zero at the start of inflation. All four of the parachutes suffered structural damage at full inflation, therefore no data is presented for times after full inflation. In these figures the experimental and analytical total loads are shown, as well as components of the analytical load: $qC_{D_0}S_0S_r$, $\dot{m}_aV$, and $m_a\dot{V}$. By design, the experimental and analytical values of the peak load agree exactly, since k_0 was set to a value that would yield such agreement. For $0 \le t/t_{inf} < 1$, the agreement between the analytical total load and the experimental load data is fair (DTST 040) to good (DTST 071). The analysis indicated that the $qC_{D_0}S_0S_r$ term accounted for approximately 50 percent of the total load with the $\dot{m}_aV$ term being of approximately equal magnitude. The $m_a\dot{V}$ term is negative and significantly smaller in absolute value than either the $qC_{D_0}S_0S_r$ or $\dot{m}_aV$ terms. Note that the $\dot{m}_aV$ term depends on the time derivative of S_r (see equation 4) and is very sensitive to dS_r/dt at full inflation. This implies that an accurate determination of dS_r/dt at full inflation is critical. Unfortunately, determining an exact value of this derivative at full inflation was difficult. The S_r vs time data obtained from the digital video camera had to be splined to obtain a smooth function $S_r(t)$. However, this splining process is not unique; various equally valid smooth functions $S_r(t)$ can be derived from the same digital video data. This non-uniqueness becomes even more critical for dS_r/dt at full inflation since S_r increases rapidly at this point. An additional source of uncertainty in this analysis arose from the manner in which the velocity and dynamic pressure were determined. These quantities were derived by integration of the accelerometer data. Although this was considered to be the best possible way of obtaining these quantities from the available data, concerns remained regarding accuracy. Discrepancies in the values of V and q have significant effects on the two main terms in the force calculation: $qC_{D_0}S_0S_r$ and $\dot{m}_aV$. In addition, the total angle of attack at mortar firing varies from drop to drop as shown in table 2. These issues may partially account for the varying degrees of success observed in matching the load data for $0 \le t/t_{inf} < 1$, and the range of values of k_0 obtained from these four drop tests (0.425 to 0.685) as shown in table 2.

WIND TUNNEL TESTS

Twelve tests were conducted during the wind tunnel test series. These tests were denoted WTMD 1 through WTMD 12, where WTMD stands for Wind Tunnel Mortar Deployed.

TEST PARACHUTES

Construction details for each of the parachutes used in these tests are given in table 3. During this test series various parachute designs were investigated. Among the parachute parameters varied were band height, constrained vent diameter, fabric material, and construction technique. The objective in varying these parameters was to determine the parachute design that would yield the best combination of drag, stability, and inflation reliability while meeting the structural design and packed volume requirements. After structural problems were encountered with the parachutes tested in drop tests DTST 040, 049, 050, and 071, the MER parachute had to be re-designed. The wind tunnel tests described here were part of the re-design and final structural qualification. All parachutes were pressure-packed to a density of approximately 45 lb/ft^3. The final parachute design, selected for the MER mission, was tested in WTMD 11 and 12. The parachute used

for WTMD 11 was an engineering prototype, while that used for WTMD 12 was a qualification test article built concurrently with the flight lot.

TEST SETUP AND PROCEDURES

The final structural qualification test series was conducted in the NFAC 80- by 120-foot wind tunnel with full-scale parachutes. These tests used an existing facility strut and ball-and-socket joint that allowed the placing of test-specific hardware near the centerline of the test section. The test-specific hardware consisted of a mounting system that held the mortar, load cell, and two aft-facing digital video cameras. This mounting system was counterbalanced and allowed to pivot on the ball-and-socket joint on top of the strut. By allowing the mounting system to pivot, side loads on the load cell were reduced to a minimum, enhancing measurement accuracy and reducing the possibility of load cell failure due to side loads. In addition, attaching the two aft-facing digital video cameras directly to the pivoting mounting system enabled them to track the parachute at all times. Figure 10 shows the mounting system during final installation on top of the strut (note the two aft-facing digital video camera housings on either side of the mortar barrel). During testing, the mortar was held at a 10° angle above horizontal by a set of Kevlar™ break-ties. These break-ties held the mortar aligned during firing. By pointing the mortar up by 10°, the parachute pack traced a parabolic trajectory which placed the parachute directly downstream of the mortar at the onset of the inflation. As the parachute inflated, and the drag force increased to approximately 1,000 lb, the break-ties released, allowing the mounting system to pivot freely. The test procedure involved increasing the wind tunnel airspeed until the desired dynamic pressure was reached, starting the data acquisition system, and firing the mortar which resulted in the deployment and inflation of the parachute. Once inflation was completed, the data acquisition system was turned off and the airspeed reduced. At airspeeds below 17.5 knots, personnel were allowed in the tunnel test section to inspect the parachute and gather it as the airspeed was reduced to zero. Figure 11 shows the strut, mounting system, and inflated parachute.

The instrumentation most relevant to this study are the load cell, dynamic pressure transducer, and aft-facing digital video cameras. The load cell was calibrated over a range from –16,000 to 35,000 lb and had an estimated accuracy of ±35 lb. Since the load cell tracked the parachute (because it was mounted on a pivoting mechanism), it measured the parachute tangential force, not the drag force. However, earlier wind tunnel tests with sub-scale models performed at the NASA Langley Research Center Transonic Dynamics Tunnel[15] indicated that the trim angle of attack for this type of DGB parachute was less than 10°. Thus, in the present investigation, the error induced by not differentiating between the tangential and drag forces (or their coefficients) was negligibly small and was therefore ignored. The force reading from the load cell during inflation was an accurate measurement of F_p. Dynamic pressure was measured approximately 150 ft upstream of the parachute canopy, yielding q_∞. With the transducers mounted close to the pitot-static tube, the lag in the q_∞ measurement was considered to be negligible. Both the load cell and dynamic pressure measurements were sampled at 200 Hz by the data acquisition system. The aft-facing digital video cameras recorded at 30 frames per second. Data from these video cameras was used to determine S_r. A more thorough description of the wind tunnel test setup and its operation is presented in reference 5.

RESULTS AND ANALYSES

Figure 12 shows a typical example of the data obtained during a wind tunnel test. From the load cell data, key points in the deployment and inflation sequence can be determined: mortar firing followed by the peak mortar firing reaction load, line stretch followed by the peak snatch load, the start of inflation, and the peak load. The term "start of inflation" is used to refer to the point where the load is at a minimum following the snatch load. This point provided a clearly identifiable point to start the inflation analyses. From figure 12 it can also be seen that q_∞ is essentially constant during parachute inflation. However, the effective dynamic pressure, q_{eff}, increases during inflation to a value 18 percent greater than q_∞ at full inflation for this test. This is due to the wind tunnel blockage as discussed earlier; q_{eff} is calculated from equation 8. The curve for S_r indicates that the peak load occurred at full inflation to within the accuracy of the time tag in the digital video camera from which it is derived. The digital video data for S_r was smoothed by a spline for plotting and use in the analyses that followed. Note that the plateau observed in the drop test load curves (see figures 6 through 9) was also present in the wind tunnel test results. Again, the hesitation in the inflation, as shown by the S_r curve, is the presumed reason for this plateau.

A summary of the wind tunnel test results is presented in table 4. Mortar performance and parachute extraction from its deployment bag are consistent across tests, as can be seen from the times from mortar firing (MF) to line stretch (LS), and from mortar firing to the start of inflation (SI). The peak mortar firing reaction load had a range from –9,091 to –11,150 lb, and the peak snatch load a range from 867 to 1,450 lb.

Note that these were transient loads, the 200 Hz sampling rate limited the accuracy to which these peak loads could be resolved. The non-dimensional inflation distance of the parachutes (i.e., last row of table 4) varied greatly. During test WTMD 2 the parachute partially inflated, and assumed a stable state that was not fully inflated. While lowering the wind tunnel airspeed, the parachute ultimately achieved a fully inflated shape at an airspeed significantly lower than that at mortar firing. The data at peak load shown in table 4 for WTMD 2 was at this lower airspeed. In test WTMD 4 the parachute again assumed a stable state that was not fully inflated, but eventually inflated fully. This was reflected in the non-dimensional distance required to inflate the parachute in this test: 39.09. No clear connection could be established between the parachute geometry and the inflation distance across the parachutes tested. For otherwise identical parachutes however, decreasing the vent area decreased the non-dimensional inflation distance (compare tests WTMD 7 and 8 against WTMD 9 and 10). Blockage of the wind tunnel test section increased q_{eff} by 14 to 18 percent above q_∞ at peak load, depending on the parachute drag coefficient and nominal area. Blockage can be assessed by the value of q_{eff}/q_∞. For all tests q_∞ was essentially constant during inflation.

The peak loads (excluding test WTMD 2) ranged from 15,336 to 29,442 lb. In all cases, peak load occurred at full inflation. An interesting parameter to study is C_x, the opening load factor, which is given by:

$$C_x = \frac{\text{Peak Load}}{q_{eff} C_{D_0} S_0} \tag{10}$$

This is the ratio of the peak load generated by the parachute at full inflation (due to both unsteady and steady components) to the steady state force at an equivalent dynamic pressure. As can be seen from table 4, the values of C_x lie within the range from 1.57 to 1.86 across all parachutes tested. Figure 13 shows C_x plotted vs q_{eff} for all tests except WTMD 2. As can be seen, C_x is shown to be dependent on q_{eff}. The *Recovery System Design Guide*[17] cites a value of ~1.30 for DGB parachutes (p. 76). It is possible that this value was generated using data from the numerous high-altitude supersonic flight tests of DGB parachutes in the 1960's and 1970's where apparent mass effects were smaller. A more interesting way of looking at the peak load test data is by normalizing it to a common parachute drag coefficient and nominal area through the equation:

$$\text{Peak Load}_{\text{normalized}} = \text{Peak Load}\,\frac{\left(C_{D_0} S_0\right)_{\text{normalized}}}{C_{D_0} S_0} \tag{11}$$

In the present analysis a value of 727.5 ft^2 was used for $\left(C_{D_0} S_0\right)_{\text{normalized}}$. This is the value of $C_{D_0} S_0$ for the parachute used in the final qualification test (WTMD 12). The normalized peak load is plotted vs q_{eff} in figure 14. As can be seen, a good correlation can be established between the normalized peak load and q_{eff}. A linear regression through the data yielded a fit with a maximum residual of –1,207 lb, and a 95 percent confidence interval for individual predictions (i.e., future tests) of approximately ±2,000 lb about the linear regression. From the standpoint of loads predictions for similar wind tunnel tests, this figure yielded two interesting conclusions. First, for tests with DGB parachutes, the linear fit shown in figure 14 could be used to estimate the peak load during similar wind tunnel tests to a useful level of accuracy. Second, for tests with other parachute types, a similar relationship between the normalized peak load and q_{eff} might be generated from the results of a few tests. Such a correlation, if it is generated with data at lower peak loads, can help in determining the value of q_{eff} required to achieve higher peak loads with less risk of overload. During the present investigation, the peak loads for the first few tests were predicted using data from the drop test program and analyses based on the apparent mass model. After a few data points were acquired, an empirical fit similar to the one shown in figure 14 was generated to predict the peak load of later tests. This empirical fit was updated as additional data was acquired.

Data from all wind tunnel tests were analyzed using the apparent mass model discussed earlier. Results for three of these analyses are presented here. The three tests chosen for presentation are WTMD 5, 11, and 12. Test WTMD 5 was chosen because the parachute used in this test was the same as that used during drop test DTST 038 and thus provided a good comparison between the drop tests and the wind tunnel tests. Tests WTMD 11 and 12 were chosen because they were the final qualification tests for the MER parachute, using identical parachutes at the same test condition. The parachute used in WTMD 11 was an engineering prototype; the parachute used in WTMD 12 was a qualification unit fabricated concurrently with the flight parachutes. Figure 12 shows the key parameters for test WTMD 5; figures 15 and 16 present the same data for tests WTMD 11 and 12. A comparison of figures 15 and 16 indicates that the test conditions and results for tests WTMD 11 and 12 are almost identical, showing good test-to-test repeatability. Figures 17, 18, and 19 show the experimental results and analytical reconstructions (using the apparent mass model) for tests WTMD 5, 11, and 12. Note that the results are plotted against non-dimensional time, t/t_{inf}, where t_{inf} is

the inflation time from the start of inflation to full inflation (also peak load for the wind tunnel tests) and the time t is zero at the start of inflation. For test WTMD5 (figure 17) no data is shown for $t/t_{inf} > 1$ since the parachute was damaged at full inflation voiding further data analyses. In these figures the experimental and analytical total loads are shown, in addition to the components of the analytical load: $q_{eff} C_{D_0} S_0 S_r$, $\dot{m}_a V_{eff}$, and $m_a \dot{V}_{eff}$. After peak inflation the $\dot{m}_a V_{eff}$ and $m_a \dot{V}_{eff}$ terms are negligible, and the drag is mainly due to $q_{eff} C_{D_0} S_0$. As with the analysis of the drop test data, the wind tunnel experimental and analytical values of the peak load agree exactly since k_0 was set to a value that would yield such agreement. For $0 \le t/t_{inf} < 1$, the analytical total load prediction agreed well with the experimental data for test WTMD 5; the agreement was only fair for tests WTMD 11 and 12, with a tendency for the analysis to overpredict the total load. The analysis indicated that the $q_{eff} C_{D_0} S_0 S_r$ term dominated the load calculation. However, the $\dot{m}_a V_{eff}$ provided a significant contribution to the total load at full inflation. The $m_a \dot{V}_{eff}$ term was positive and accounted for only a small fraction of the total load; not more than a few hundred pounds at full inflation. Again note that the $\dot{m}_a V_{eff}$ term depends on the time derivative of S_r (see equation 4) and is very sensitive to dS_r/dt at full inflation. The remarks made in the drop test section regarding the accuracy of dS_r/dt and its effect on the analysis results also apply to the wind tunnel test. This issue may account for the varying degrees of success observed in matching the load data for $0 \le t/t_{inf} < 1$ and the range of values of k_0 obtained from the eleven valid wind tunnel tests (0.420 to 0.640). Note that concerns regarding uncertainties in the velocity (airspeed) and dynamic pressure in the discussion of the drop test data are not applicable to the wind tunnel test data. The variation in k_0 obtained from the wind tunnel test data analyses also reflects the differences in parachute geometries during the wind tunnel test series. For the cases examined here in detail, k_0 was 0.420 for test WTMD 5, 0.597 for test WTMD 11, and 0.589 for test WTMD 12.

COMPARISON OF DROP AND WIND TUNNEL TEST DATA AND ANALYSES

The parachute used in wind tunnel test WTMD 5 was of the same size and geometry as those used in the drop test series. This provided the opportunity to make a direct comparison of the results of drop and wind tunnel tests. The drop tests considered in this discussion are DTST 040, 049, 050, and 071. These parachute drop tests reached peak load at full inflation, as did wind tunnel test WTMD 5. The data used for most of the following comparisons can be found in table 2 for the drop tests and table 4 for the wind tunnel test.

The non-dimensional inflation distance for the four drop tests varied from 7.93 to 9.12 with an average of 8.60. The value for wind tunnel test WTMD5 was 10.27 - above the range and average value for the drop tests. Calculated values of k_0, for the drop tests considered here varied from 0.425 to 0.685 with an average of 0.534. The calculated value of k_0 for wind tunnel test WTMD 5 was 0.420 - at the lower end of the range and below the average value for the drop tests. In comparing values of the opening load factor, C_x, the dynamic pressure at full inflation should be as close as possible since, as shown in figure 13, C_x is dependent on this parameter. Drop test DTST 071 was chosen for comparison against wind tunnel test WTMD5 because these two tests had similar values of q and q_{eff} at full inflation (q = 15.1 psf for DTST 071; q_{eff} = 14.5 for WTMD 5). The opening load factor for tests DTST 071 and WTMD 5 were calculated to be 1.85 and 1.75, respectively – within 6 percent of one another. The observed discrepancies in these quantities (i.e., inflation distance, k_0, and C_x) may be within the test-to-test variation and/or the accuracy of the drop test measurement capability. However, these differences may also indicate problems with the apparent mass model as currently implemented or reflect differences in the inflation of the parachutes due to the test method. The limited amount of tests that can be compared directly (i.e., one wind tunnel test and four drop tests) makes it impossible to make definitive statements without further analysis.

Figure 20 shows the non-dimensional inflation curves (i.e., S_r vs t/t_{inf}) for the four drop tests and wind tunnel test WTMD 5. Since the purpose was to compare drop and wind tunnel tests, inflation curves for all drop tests are shown as dashed lines and the wind tunnel test is shown as a solid line. All non-dimensional curves are very similar and exhibit the same hesitation in the inflation process at some point between t/t_{inf} = 0.6 and 0.9. The similarity in these curves indicates that the parachute inflation profile, as given by S_r, does not differ significantly between drop and wind tunnel tests.

CONCLUDING REMARKS

Parachute opening load test results for various DGB parachutes have been presented. These test results were obtained from both drop tests and wind tunnel tests. Of these two test methods the wind tunnel tests yielded more accurate and repeatable data.

Applying the apparent mass model to opening loads data from drop tests and wind tunnel tests yielded insights on the nature of these loads. Although reconstructions of specific tests gave results of reasonable accuracy, the use of this model for predictive analyses was not accurate enough for setting test conditions for either the drop or wind tunnel tests. Based on a few test results, a simpler empirical model was able to predict opening loads for wind tunnel tests to the required accuracy. However, this simple model is not applicable to drop tests because the dynamic pressure at full inflation is not known apriori.

ACKNOWLEDGEMENTS

The authors would like to express their appreciation to the Mars Exploration Rover project, and in particular to Robin Bruno, Adam Steltzner, and Wayne Lee of the NASA Jet Propulsion Laboratory for their support of this work.

REFERENCES

1) Witkowski, A. and Bruno, R., "Mars Exploration Rover Parachute Decelerator System Program Overview," AIAA Paper 2003-2100, 2003.

2) Steltzner, A., Lee, W., Bruno, R., and Desai, P., "The Mars Exploration Rovers Entry Descent and Landing Phase and the Use of Aerodynamic Decelerators," AIAA Paper 2003-2125, 2003.

3) Taeger, Y. and Witkowski, A., "A Summary of Dynamic Testing of the Mars Exploration Rover Parachute Decelerator System," AIAA Paper 2003-2127, 2003.

4) Way, D., Desai, P., Engelung, W., Cruz, J., and Hughes, S., "Design and Analysis of the Drop Test Vehicle for the Mars Exploration Rover Parachute Structural Tests," AIAA Paper 2003-2138, 2003.

5) Zell, P., Cruz, J., and Witkowski, A., "Structural Testing of Parachutes in the National Full-Scale Aerodynamics Complex 80- by 120-foot Wind Tunnel at NASA Ames," AIAA Paper 2003-2130, 2003.

6) Gillis, C. L., "The Viking Decelerator System – An Overview," AIAA Paper 73-442, 1973.

7) Fallon II, E. J., "System Design Overview of the Mars Pathfinder Parachute Decelerator Subsystem," AIAA Paper 97-1511, 1997.

8) Witkowski, A., "Mars Pathfinder Parachute System Performance," AIAA Paper 99-1701, 1999.

9) Brecht, J. P., Pleasants, J. E., and Mehring, R. D., "The Viking Mortar: Design, Development, and Flight Qualification," AIAA Paper 73-458, 1973.

10) Vasas, R. and Styner, J., "Mars Exploration Rover Parachute Mortar Deployer Development," AIAA Paper 2003-2137, 2003.

11) Steltzner, A., Bruno, R., Mitcheltree, R., and Cruz, J., "Opportunities and Limitations in Low-Earth Subsonic Testing and Qualification of Extraterrestrial Supersonic Parachute Designs," AIAA Paper 2003-2135, 2003.

12) McEwan, A. J., "An Investigation of Parachute Opening Loads, and a New Engineering Method for their Determination," AIAA Paper 70-1168, 1970.

13) McBride, D. D., "Orbiter Drag Chute Stability Test in the NASA/Ames 80 x 120 Foot Wind Tunnel," Sandia Report SAND93-2544, 1994.

14) Macha, J. M. and Buffington, R. J., "Wall-Interference Corrections for Parachutes in a Closed Wind Tunnel," *Journal of Aircraft*, Vol. 27, No. 3, 1990, pp. 320-325.

15) Cruz, J., Mineck, R., Keller, D., and Bobskill, M., "Wind Tunnel Testing of Various Disk-Gap-Band Parachutes," AIAA Paper 2003-2129, 2003.

16) Desai, P., Schofield, J., and Lisano, M., "Flight Reconstruction of the Mars Pathfinder Disk-Gap-Band Parachute Drag Coefficient," AIAA Paper 2003-2126, 2003.

17) Ewing, E. G., Bixby, H. W., and Knacke, T. W., "Recovery System Design Guide," AFFDL-TR-78-151, 1978.

Table 1 – Drop Test Parachute Information.

	DTST 037	DTST 038	DTST 040	DTST 049	DTST 050	DTST 071
Type	MPF	MPF	MPF	MPF	MPF	MPF
Serial Number	622809	622810	622813	622812	622811	622814
Test Date	5/5/2002	5/8/2002	6/13/2002	6/15/2002	6/17/2002	6/19/2002
D_0 (ft)	50.1	49.7	50.1	49.8	49.9	50.1
S_0 (ft^2)	1971	1940	1969	1945	1958	1969
D_D/D_0	0.616	0.623	0.618	0.615	0.613	0.617
$D_{V,c}/D_0$	0.0627	0.0634	0.0626	0.0631	0.0630	0.0628
D_B/D_0	0.568	0.573	0.568	0.572	0.573	0.568
H_B/D_0	0.233	0.230	0.233	0.231	0.231	0.233
H_G/D_0	0.0377	0.0380	0.0378	0.0380	0.0378	0.0378
L_S/D_0	1.67	1.69	1.67	1.68	1.68	1.67
$A_{V,c}/A_D$	0.0104	0.0107	0.0103	0.0105	0.0105	0.0104
$\lambda_{g,c}$ (%)	9.35	9.49	9.36	9.49	9.45	9.36

Note: See figure 1 and/or the *Symbols and Acronyms* section for the meaning and definitions of the various symbols. All dimensions from as-built measurement samples.

Table 2 – Summary of Drop Test Results.

	DTST 037	DTST 038	DTST 040	DTST 049	DTST 050	DTST 071
DTV Weight	3,011	2,988	7,900	7,900	7,900	7,900
Time Release to MF	4.773	4.758	3.100	2.320	1.830	1.670
Time MF to LS (s)	0.765	0.750	0.800	0.835	0.755	0.815
Time MF to SI (s)	1.005	0.965	0.966	1.180	1.035	0.890
Time LS to SI (s)	0.240	0.215	0.166	0.345	0.280	0.075
Time MF to PL (s)	3.000	2.460	3.675	4.295	4.390	4.180
Time SI to PL (s)	1.995	1.495	2.709	3.115	3.355	3.290
Time SI to FI (s)	3.050	2.265	2.709	3.115	3.355	3.290
Total Angle of Attack at MF	4.3°	1.4°	9.1°	17.1°	24.8°	17.4°
Peak MF Reaction Load (lb) (see note 5)	-13,277	-7,840	-10,381	-2,392	-6,376	-10,086
Peak Snatch Load (lb) (see note 5)	992	1,012	856	795	610	926
Peak Load (lb)	12,889	14,529	30,027	29,665	25,329	22,153
Load at FI (lb)	10,134	12,729	30,027	29,665	25,329	22,153
q at PL (psf)	34.1	29.3	20.8	17.9	16.5	15.1
Percent Inflation at PL (see note 2)	66	66	100	100	100	100
q at FI (psf)	13.8	10.2	20.8	17.9	16.5	15.1
C_{D_0}	0.41	0.41	0.41	0.41	0.41	0.41
$qC_{D_0}S_0$ at PL (lb)	See note 4	See note 4	16,792	14,274	13,246	12,190
$\frac{qC_{D_0}S_0}{\text{Peak Load}}$ at PL	See note 4	See note 4	0.559	0.481	0.523	0.542
C_x	See note 4	See note 4	1.79	2.08	1.91	1.85
k_0	See note 4	See note 4	0.425	0.685	0.501	0.525
Inflation Distance/D_0	11.07	7.69	8.57	9.12	8.76	7.93

Notes:

1) Acronyms: MF – Mortar Firing; LS – Line Stretch; SI – Start of Inflation; PL – Peak Load; FI – Full Inflation.
2) Percent Inflation at PL = 100 • (Time SI to PL/Time SI to FI).
3) C_{D_0} is not a test result; it is the assumed value used for the analyses and listed here for convenience. The value of C_{D_0} was determined from the results of wind tunnel tests,[15] and reconstruction of the Mars Pathfinder entry.[16]
4) Certain quantities were not calculated for DTST 037 and 038 because peak load did not occur at full inflation.
5) Data acquisition rate (200 Hz) and vehicle mass limited the accuracy of measurement of these impulsive/transient loads.

Table 3 – Wind Tunnel Test Parachutes Information.

	WTMD 1	WTMD 2	WTMD 3	WTMD 4	WTMD 5	WTMD 6	WTMD 7	WTMD 8	WTMD 9	WTMD 10	WTMD 11	WTMD 12
Type	1.6 Hybrid	1.6 Viking	1.8 Viking	1.8 Viking	MPF	1.8 Viking	1.8 MPF	1.8 MPF	1.8 MPF	1.8 MPF	1.8 MPF	1.8 MPF
Serial Number	622808	622905	622910	622923	622810	622924	622931	622930	622931	622930	623194	623196
Test Date	9/12/2002	9/17/2002	9/19/2002	9/25/2002	9/25/2002	9/27/2002	10/10/2002	10/10/2002	10/30/2002	10/30/2002	10/30/2002	1/15/2003
D_0 (ft)	44.6	43.2	44.5	44.4	49.7	44.5	43.4	43.3	43.4	43.3	46.3	46.3
S_0 (ft^2)	1562	1466	1555	1548	1940	1555	1479	1473	1479	1473	1684	1684
D_D/D_0	0.693	0.643	0.613	0.612	0.623	0.614	0.628	0.631	0.628	0.631	0.63	0.633
$D_{V,c}/D_0$	0.0705	0.0713	0.0722	0.0726	0.0634	0.0723	0.0359	0.036	0.0638	0.064	0.0643	0.0644
D_B/D_0	0.639	0.642	0.602	0.604	0.573	0.602	0.578	0.577	0.578	0.577	0.588	0.586
H_B/D_0	0.161	0.187	0.215	0.215	0.230	0.216	0.221	0.221	0.221	0.221	0.216	0.216
H_G/D_0	0.0421	0.0427	0.0431	0.0433	0.038	0.043	0.0383	0.0385	0.0383	0.0385	0.0383	0.0382
L_S/D_0	1.88	1.74	1.77	1.77	1.69	1.77	1.82	1.82	1.82	1.82	1.70	1.70
$A_{V,c}/A_D$	0.0103	0.0123	0.0139	0.0141	0.0104	0.0139	0.0033	0.0033	0.0103	0.0103	0.0104	0.0104
$\lambda_{g,c}$ (%)	11.74	11.48	11.02	11.09	9.49	10.99	9.38	9.44	9.66	9.72	9.77	9.74

Notes

1) See figure 1 and/or the *Symbols and Acronyms* section for the meaning and definitions of the various symbols. All dimensions from as-built measurement samples.
2) "Type" is the name used by the MER team to denote the various canopy geometries. The number denotes the height of the band as a multiple of that used by the Viking parachute. MPF is the geometry that was used by the Mars Pathfinder mission. The Viking and MPF parachutes have differences in the ratios of the vent area to the disk area, the gap height to the nominal diameter, and the band diameter to the disk diameter.
3) The parachute tested in WTMD1 (Serial Number 622808) was of a hybrid Viking/MPF type.
4) The parachute used for WTMD 5 was the same as that used for drop test DTST 038.
5) Tests WTMD 7 through 10 used parachutes with a fabric vent cap to reduce the constrained vent diameter and area.
6) Tests WTMD 7 and 9 used the same parachute with different vent caps. Tests WTMD 8 and 10 used the same parachute with different vent caps.
7) The vent diameter was constrained by the vent cords in the parachutes used for WTMD 1 through 6, 11, and 12. The vent diameter was constrained by fabric vent caps for tests WTMD 7 through 10.

Table 4 – Summary of Wind Tunnel Test Results.

	WTMD 1	WTMD 2	WTMD 3	WTMD 4	WTMD 5	WTMD 6	WTMD 7	WTMD 8	WTMD 9	WTMD 10	WTMD 11	WTMD 12
Time MF to LS (s)	0.820	0.705	0.765	0.750	0.805	0.750	0.725	0.735	0.755	0.760	0.755	0.725
Time MF to SI (s)	1.130	0.945	1.030	1.045	1.100	1.045	0.960	0.975	0.995	1.000	1.000	0.975
Time LS to SI (s)	0.310	0.240	0.265	0.295	0.295	0.295	0.235	0.240	0.240	0.240	0.245	0.250
Time MF to PL (s)	5.850	NA	6.650	14.410	6.020	4.185	4.315	4.250	5.610	7.370	4.090	4.115
Time SI to PL (s)	4.720	NA	5.620	13.365	4.920	3.140	3.355	3.275	4.615	6.370	3.090	3.140
Peak MF Reaction Load (lb) (see note 6)	-9,267	-11,102	-10,512	-10,501	-9,091	-10,311	-9,759	-9,198	-10,208	-9,572	-9,587	-11,150
Peak Snatch Load (lb) (see note 6)	904	1,450	867	1,158	708	960	1,167	1,295	1,183	917	1,107	1,008
Peak Load (lb)	15,336	4,841	20,597	25,201	19,507	17,356	23,023	29,442	26,441	22,270	25,363	25,289
ρ (slugs/ft^3)	0.002344	0.002342	0.002247	0.002341	0.002294	0.002306	0.002345	0.002338	0.002366	0.002336	0.002340	0.002399
V_∞ at PL (ft/s)	89.9	53.3	120.6	129.6	103.6	103.9	129.9	149.0	139.6	129.5	122.4	120.6
V_{eff} at PL (ft/s)	97.3	57.4	129.2	138.8	112.5	111.4	138.7	159.0	149.1	139.2	132.0	130.1
q_∞ at PL (psf)	9.47	3.33	16.34	19.66	12.32	12.45	19.77	25.94	23.06	19.85	17.53	17.46
q_{eff} at PL (psf)	11.10	3.86	18.76	22.56	14.52	14.30	22.55	29.56	26.30	22.62	20.38	20.30
q_{eff}/q_∞ at PL	1.171	NA	1.149	1.148	1.178	1.149	1.140	1.140	1.140	1.140	1.163	1.163
C_{D_0}	0.486	0.486	0.432	0.432	0.405	0.432	0.432	0.432	0.432	0.432	0.432	0.432
$q_{eff} C_{D_0} S_0$ at PL (lb)	8,246	2,747	12,396	14,842	11,146	9,449	14,193	18,524	16,552	14,172	14,534	14,477
$\frac{q_{eff} C_{D_0} S_0}{\text{Peak Load}}$ at PL	0.538	0.567	0.602	0.589	0.571	0.544	0.616	0.629	0.626	0.636	0.575	0.572
C_x	1.86	1.76	1.66	1.70	1.75	1.84	1.62	1.59	1.60	1.57	1.74	1.75
k_0	0.634	NA	0.566	0.640	0.420	0.509	0.513	0.498	0.673	0.612	0.597	0.589
Inflation Distance/D_0	9.52	NA	15.25	39.09	10.27	7.34	10.06	11.29	14.87	19.09	8.18	8.19

Notes:

1) Acronyms: MF – Mortar Firing; LS – Line Stretch; SI – Start of Inflation; PL – Peak Load.
2) V_∞ is the airspeed well upstream of the parachute canopy. It is derived from q_∞ through the equation $V_\infty = \sqrt{2q_\infty/\rho}$.
3) NA – Not Applicable; used for certain rows for test WTMD 2. This parachute failed to achieve full inflation at the test dynamic pressure. However, it finally inflated at a highly reduced dynamic pressure and airspeed.
4) C_{D_0} is not a test result; it is the assumed value used for the analyses and listed here for convenience. The values of C_{D_0} were determined from the results of previous drop tests,[3] wind tunnel tests,[15] and reconstruction of the Mars Pathfinder entry.[16] Interpolations were used as necessary.
5) The nondimensional inflation distance is based on calculations using V_{eff}.
6) Data acquisition rate (200 Hz) limited the accuracy of measurement of these impulsive/transient loads.

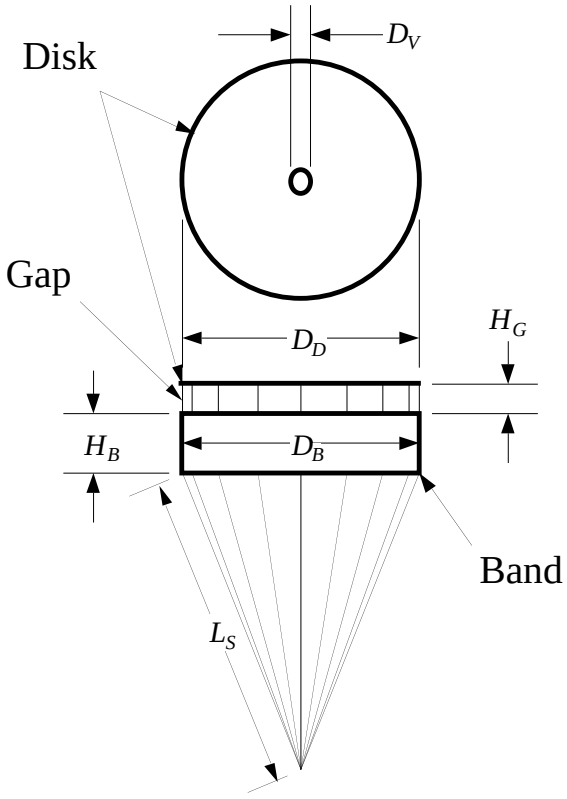

Figure 1 – Key geometric parameters for a DGB parachute.

Figure 2 – Drop test vehicle (DTV); 3,000 lb nominal weight.

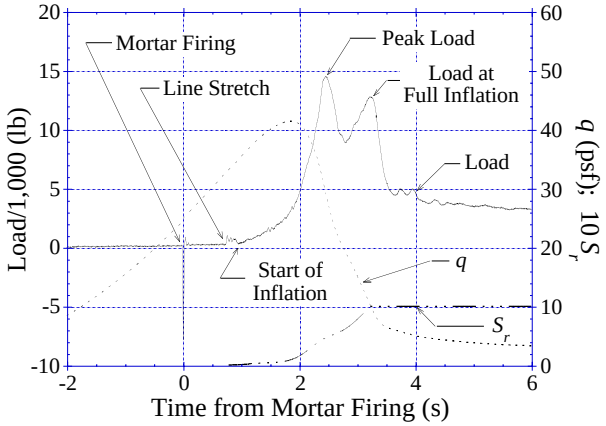

Figure 3 – Key parameters from drop test DTST 038.

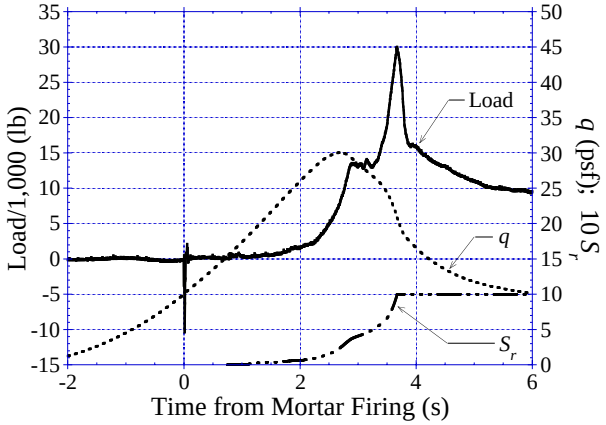

Figure 4 – Key parameters from drop test DTST 040.

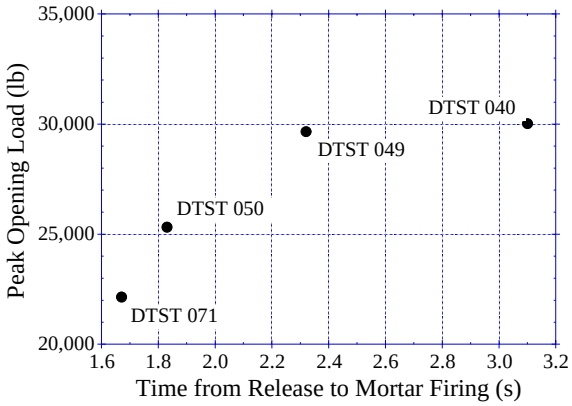

Figure 5 – Peak opening load vs time from release to mortar firing for drop tests with the 8,000 lb DTV. All peak opening loads at full inflation.

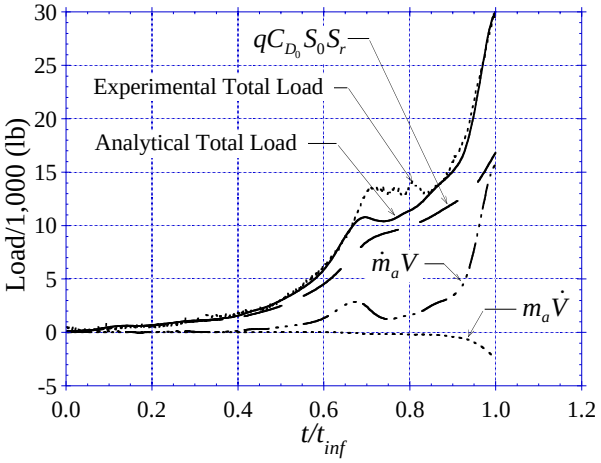

Figure 6 – Experimental total load and apparent mass model reconstruction results for drop test DTST 040.

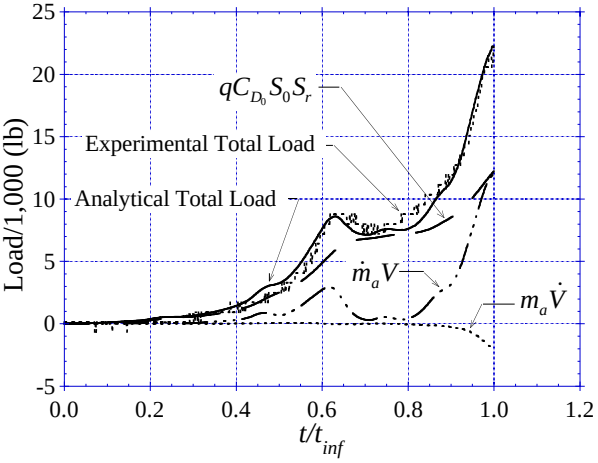

Figure 9 – Experimental total load and apparent mass model reconstruction results for drop test DTST 071.

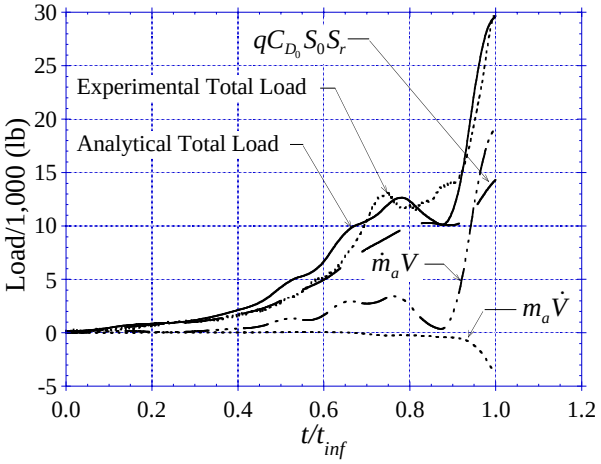

Figure 7 – Experimental total load and apparent mass model reconstruction results for drop test DTST 049.

Figure 10 – Mounting system on top of the strut in the 80- by 120-foot wind tunnel.

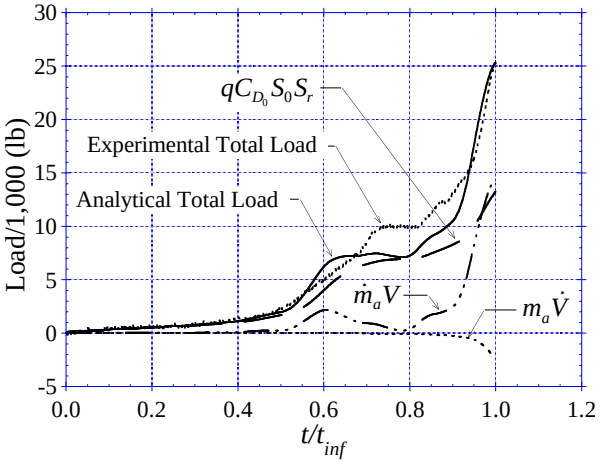

Figure 8 – Experimental total load and apparent mass model reconstruction results for drop test DTST 050.

Figure 11 – Deployed full-scale parachute being inspected in the 80- by 120-foot wind tunnel.

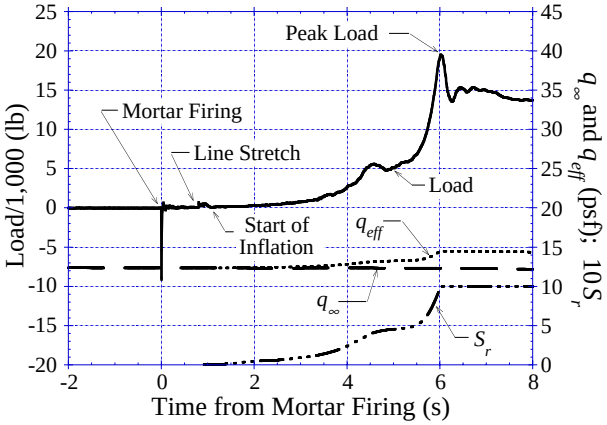

Figure 12 – Key parameters from wind tunnel test WTMD 5.

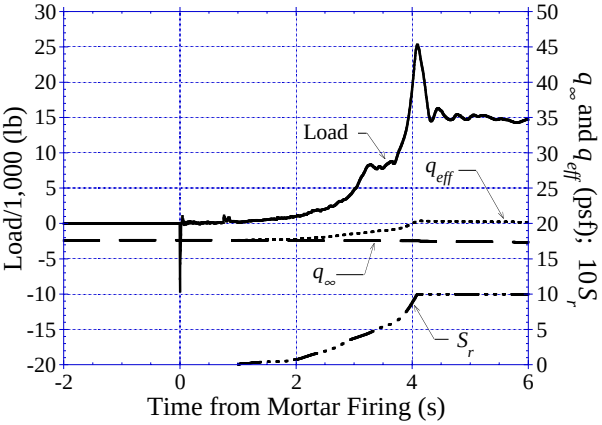

Figure 15 – Key parameters from wind tunnel test WTMD 11.

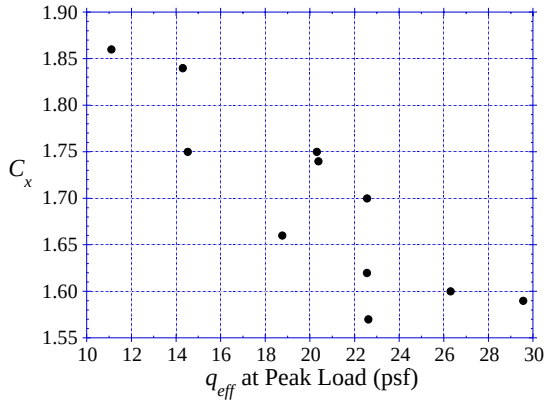

Figure 13 – C_x vs q_{eff} at peak load for all wind tunnel tests except WTMD 2.

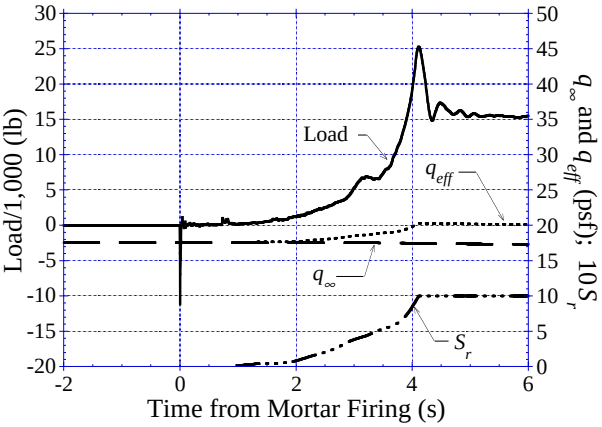

Figure 16 – Key parameters from wind tunnel test WTMD 12.

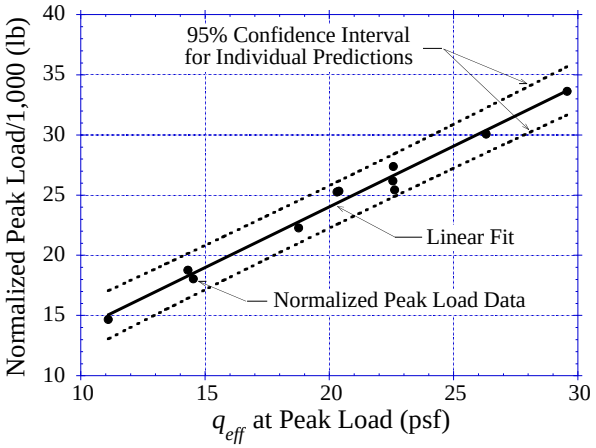

Figure 14 – Normalized peak load vs q_{eff} at peak load for all wind tunnel tests except WTMD 2.

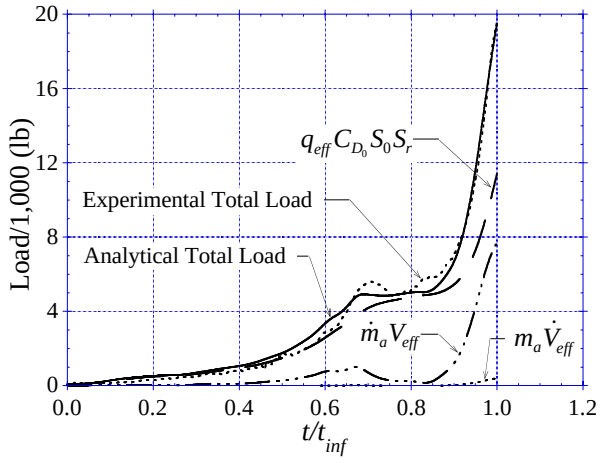

Figure 17 – Experimental total load and apparent mass model reconstruction results for wind tunnel test WTMD5.

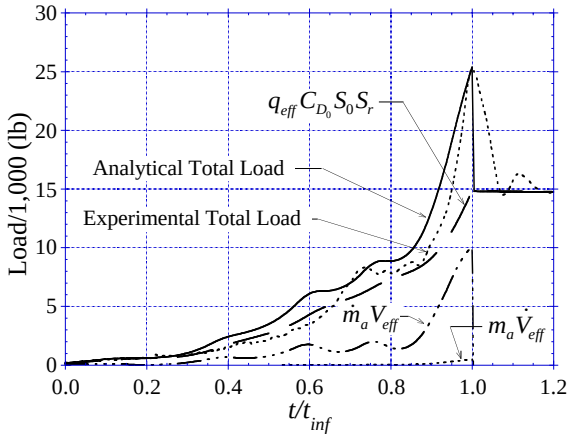

Figure 18 – Experimental total load and apparent mass model reconstruction results for wind tunnel test WTMD 11.

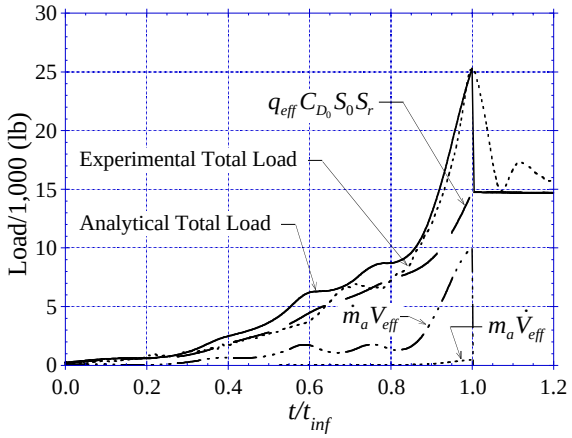

Figure 19 – Experimental total load and apparent mass model reconstruction results for wind tunnel test WTMD 12.

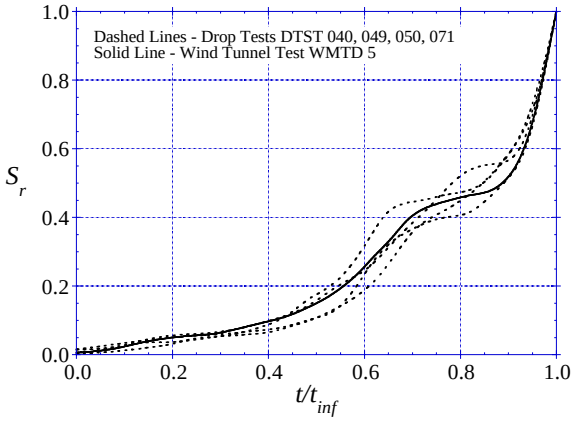

Figure 20 – Nondimensional inflation curves for drop tests DTST 040, 049, 050, 071, and wind tunnel test WTMD 5.